

## DRAFT: LAFAD Hard Ceramic and Cermet Coatings for Erosion Protection of Turbomachinery Components

Vladimir Gorokhovskiy<sup>1</sup>, Chris Bowman<sup>1</sup>, John Wallace<sup>1</sup>, Dave VanVorous<sup>1</sup>, John O'Keefe<sup>1</sup>, Victor Champagne<sup>2</sup>, Marc Pepi<sup>2</sup>, Widen Tabakoff<sup>3</sup>

<sup>1</sup>Arcomac Surface Engineering, LLC

<sup>2</sup>US Army Research Laboratory

<sup>3</sup>University of Cincinnati

### ABSTRACT

To mitigate costly surface damage, compressor blades are coated with materials that resist corrosion and resist wear from particle impact. Large Area Filtered Arc Deposition (LAFAD) technology has demonstrated the capability of depositing relatively thick cermet coatings with microlaminated architectures forming a stack of metallic/ceramic bi-layers. These coatings have nearly defect-free morphology and an extremely smooth surface with high surface energy, which improves the aerodynamics of airfoils. Yet, the deposition process can be carried out at a speed that produces coatings sufficiently thick to provide long life protection from particle damage at a cost-effective production rate. The basic mechanical properties and erosion resistance of LAFAD microlaminated cermet coatings deposited on Ti6Al4V and 17-4PH steel substrates have been investigated as a function of coating composition and architecture.

### INTRODUCTION

Gas turbine engines operating in arid environments suffer significant wear from ingested sand that causes erosion damage to various components [1-4]. Damage caused by solid particle impact reduces the engine life as well as engine power and efficiency, and results in high engine maintenance costs [1]. This is a very expensive problem for commercial airlines with their current high fuel costs. It is a particularly serious problem for military aircraft and turbine powered armored vehicles that must operate in severe dust and blowing sand environments. Helicopter engines are especially susceptible to large amounts of dust and sand ingestion during hover, takeoff, and landing while the rain erosion due to interaction with water droplets at near sonic speeds imposes additional difficult problem on durability of compressor blades, vanes and helicopter rotorblades as well as power generation gas turbines. In the case of helicopter rotor blades, the size and characteristic impact velocity of the particulate flow are several times larger than that of rotating components of turbine engines due to the absence of any protective filters, which are now installed by most turbine engine manufacturers [3].

Conventional erosion-protective surface treatments consist of different metal, ceramic or cermet coatings deposited by thermal spray, CVD or PVD techniques [2]. The most popular are TiN-based coatings deposited by EB-PVD, magnetron sputtering or cathodic arc evaporation techniques [1,2,5,6]. However, these coatings have growth defects, voids and porosity, which increases the surface roughness and accelerates degradation due to both development of corrosion pits and high temperature oxidation [1,7]. Hard coatings are inherently brittle and are prone to cracking and spallation under high energy and near 90° impacts; this produces the paradoxical result that

an increase in hardness can result in a decrease in wear resistance. On the other hand, tough materials are prone to cutting and micromachining wear mechanisms at low angles of impact. One solution is to combine the hard impact resistance of ceramics with the toughness of metals by forming multilayer erosion- and wear-resistant coatings [8]. Recently, nanostructured and nanocomposite coatings utilizing nano-laminated or superlattice coating architectures with superior functional properties have been developed [7,9,10]. The vapor deposition processes used for producing nanostructured coatings require metal vapor sources with increased ionization and the ability to uniformly mix the multi-elemental metal vapor flows [7]. This allows the increase in adatom mobility necessary to produce a dense fine grain morphology without voids or porosity and with a smooth surface as required by the Movchan-Demchishin-Thornton-Messier (MDTM) zone diagram [11].

The filtered cathodic arc deposition (FCAD) process can provide a fully atomized and ionized metal vapor beam with a relatively high electron temperature on the order of 3 to 5eV which contributes to an increased ionization rate of the gaseous atmosphere via electron collisions with gas atoms and molecules. The kinetic energy of the filtered arc metal ion beams exceeds the thermal energy of the FCAD plasma by an order of magnitude, ranging from 40 to 200 eV [11]. In sharp contrast to sputtering processes, the cathodic arc evaporation process (both direct arc and filtered arc) does not require a minimum background pressure of inert gas, and can generate metal vapor plasma in any reactive gas atmosphere or even in deep vacuum [11]. These properties of the FCAD process make it advantageous compared to conventional – and even ionized – magnetron sputtering processes in many applications requiring high ionization rate of the depositing metal-gaseous vapor to increase coating density and other functional properties and to eliminate or substantially reduce the defects in the coatings. The main obstacle to using conventional FCAD technology is the low productivity of this process, which restricts its usage to semiconductors, optical coatings and some ultra-thin hard coatings for bio-medical and tribological applications. On the other hand, Large Area Filtered Arc Deposition (LAFAD) technology overcomes these limitations by providing a highly productive, robust, industry-friendly process which combines the high productivity rate of conventional direct cathodic arc deposition (DCAD) and magnetron technologies, with the capability of generating a nearly 100% ionized metal-gaseous vapor plasma with large kinetic energy and with no macroparticles, droplets, multi-atom clusters or other contaminants [12-16]. The unidirectional, dual-arc LAFAD vapor plasma sources can be used as an alternative to conventional DCAD and magnetron-based processes when the high productivity and uniformity needed for most industrial applications

must be accompanied by the high ionization and high kinetic energy of an atomically clean vapor plasma. This work is dedicated to the characterization of the LAFAD process integrated into an industrial batch coating system for the deposition of erosion protection coatings for turbomachinery components.

## EXPERIMENTAL DETAILS

**Substrate Materials:** 1x1x1/8 inch square plates made either of Ti6Al4V alloy or 17-4PH stainless steel were used as test coupons for most of the experiments conducted in this work. In addition to squares, coupons made of 301 stainless steel (3"x2"x1/8") and round discs 3/4 inch in diameter x 1/8" thick made of Ti6Al4V alloy and 440A stainless steel were also used for preliminary testing and as witness coupons for evaluation of coating thickness distribution, coating composition, and basic mechanical properties.

Different surface treatments were performed prior to subjecting the samples to the LAFAD coating deposition process. The square coupons were subjected to the following four different pre-deposition treatments:

- 1.) polishing
- 2.) bead blasting
- 3.) vibratory tumbling
- 4.) bead blasting + tumbling

These treatments, which produced four different surface finishes, were used to investigate the influence of the initial surface finish on coating properties and evolution of the surface profile due to the LAFAD coating deposition process.

### LAFAD Coating Technology:

**Figure 1** shows the LAFAD-500C batch coating system layout utilizing a vacuum chamber 0.7 meters in diameter by one meter tall, equipped with a unidirectional dual arc LAFAD plasma source. The rotatable substrate turntable, 0.5 meters in diameter, is installed in the center of the coating chamber and allows for single or double rotation of the substrates that are being coated. The LAFAD plasma source consists of the plasma guide chamber with baffles installed along its walls and the exit tunnel window which is 300 mm wide by 400 mm tall. Two pairs of deflection coils are located along the opposite walls of the plasma duct chamber. When the deflection/focusing coils of the filter chamber are turned on, the vapor plasma generated by the primary DCAD sources flows into the plasma guide chamber from opposite directions and turns around the corner of the plasma guide exit tunnel toward the coating chamber. When the deflection/focusing coils of the filter chamber are turned off, an auxiliary arc discharge can be established between the primary arc cathodes of the LAFAD source and the auxiliary arc anode located in a coating chamber behind the turntable (see **Figure 1**). This discharge provides ionization and activation of the gaseous atmosphere in the main chamber, producing a highly ionized gaseous plasma during such technological stages as ion cleaning/etching, gaseous ion implantation and ionitriding/oxyinitriding/carburizing. The detailed description of this highly versatile process can be found elsewhere [12-16].

### LAFAD Coatings Characterization:

#### *Basic coating properties characterization*

Coating thickness was determined by the CALO™ wear scar spherical abrasion technique and optical micrometry to an accuracy

of  $\pm 0.1 \mu\text{m}$ . Coating hardness and Young's modulus were measured by an MTS-XP nanoindenter with a CSM module and Berkovich tip. Adhesion evaluation was performed by the Rockwell-C 145kgf indentation test according to [17]. Average coating RMS and Rz roughness were measured per ASTM B46.1 with a Veeco Dektak8 contact profilometer. Parameters for RMS measurement were as follows; 5 $\mu\text{m}$  radius stylus, 1750 $\mu\text{m}$  scan length, 250 $\mu\text{m}$  cutoff filter (waviness filter), 1 data point/ $\mu\text{m}$ . Five RMS scans were made per sample and a minimum of six samples were scanned resulting in a 30-point RMS average per unique coating type reported. Metallurgical cross-sections were prepared for selected coatings followed by SEM micro-imaging. Coating compositions were analyzed by EDS, RBS, XPS and Auger techniques.

#### *Erosion resistance testing*

Erosion testing was performed at Arcomac Surface Engineering (ASE), utilizing a FALEX F-1507 Air Jet Erosion Test Rig with the use of alumina erodent (50 $\mu\text{m}$ ) fed at 2g/min at 90° incidence and at the University of Dayton Research Institute (UDRI), where the impact velocity of 300  $\mu\text{m}$  silica erodent media did not exceed 700 fps [18]. The most aggressive erosion testing was performed at the University of Cincinnati (UC) turbo-machinery erosion laboratory. The wind tunnel erosion testing facility of the UC is well known to closely resemble the actual conditions of airfoils in the turbine engine as described elsewhere [1]. All erosion tests at UC were conducted using runway sand at speeds of 700 fps or 1200 fps. The size distribution of runway sand ranges from few microns up to 1 mm with largest fractions consisting of 250  $\mu\text{m}$  (46%) and 500 $\mu\text{m}$  (25%); its composition is 60% quartz, 26% gypsum, 12% calcite, and 2% soluble salts.

## RESULTS AND DISCUSSION

Monolithic TiN, microlaminated Ti/TiN and nano-microlaminated Ti/TiN coatings with different thicknesses and architectures deposited on steel and titanium substrates by industrial scale LAFAD process were subjected to different testing and analysis to evaluate their physical properties and resistance to erosion for turbomachinery applications.

#### *Structure, morphology and mechanical properties characterization*

Mechanical properties of relatively thin Ti/TiN multilayer coatings (thickness less than 15  $\mu\text{m}$ ) with submicron bi-periods are dependent on the bi-period ratio. It was found that increasing the metallic sublayer thickness in Ti/TiN coatings results in a dramatic decrease of the coating stress. The increase of the metallic sublayer thickness with otherwise fixed bi-layer period will also result in a decrease of the coating hardness. Typically the hardness of thin multilayer Ti/TiN coatings deposited by the LAFAD process range from 25GPa to 35GPa when the thickness of metallic sublayers in a coating architecture is reduced, which was thoroughly investigated in [12,14,19].

Based on preliminary results of testing the relatively thin TiN coatings, the next step was to evaluate LAFAD multilayer Ti/TiN cermet coatings having nearly two times greater thickness and different architectures. Five different Ti/TiN microlaminated cermet coatings designated B, C, D, E and F with slightly different total thicknesses ranging from 20 to 25  $\mu\text{m}$ , five different bi-periods and different Ti-to-TiN sublayer thicknesses were deposited by the unidirectional LAFAD vapor plasma source on titanium and steel substrates installed on the rotating turntable of the industrial coating system shown in **Figure 1**. The Ti6Al4V and 17-4PH stainless steel

substrate coupons were subjected to four different pre-deposition treatments as described above. The characteristic parameters of these coatings are presented in **Table 1**. The deposition rates of these coatings deposited at 140 amperes primary arc current ranged from 2.2 to 2.5  $\mu\text{m/hr}$  averaged over a coating deposition time of 10 to 12 hrs.

The B1 coating (**Table 1**, item B1) shown in **Figure 2** demonstrates an extremely smooth, nearly defect-free surface. This 20  $\mu\text{m}$  thick microlaminated Ti/TiN coating was produced by the unidirectional LAFAD plasma source during a ten hour deposition period. The SEM image of the cross-section of this coating, shown in **Figure 2**, shows well-defined titanium and TiN sublayers with fine columnar structure. All of the 20-25 $\mu\text{m}$  thick Ti/TiN coatings (Table 3, items B-F)) deposited by the LAFAD process exhibit low residual compressive stresses, i.e. < 1.5GPa, resulting in exceptionally good adhesive and cohesive toughness, HF1 according to classification [17], as illustrated in **Figure 2**. Low stresses in thick TiN base coatings may be explained by the role of thickness-dependent gradients of point defect density, as was recently proposed in [20]. Optimization of Ti sublayer thickness vs. TiN sublayer thickness in this microlaminated cermet coating architecture plays an important role in energy dissipation by shear deformation, which delays critical shear and tensile stress developed at the metallic/ceramic sublayer interface [12,14,20,21]. The hardness of these microlaminated coatings measured by the nanoindentation technique exhibits a relatively low value in the range from 18 to 20 GPa. This can be considered as a composite hardness created by the interaction of soft and ductile metallic sublayers with hard and brittle ceramic sublayers in the Ti/TiN microlaminated coating architecture.

When the total arc currents of the primary arc sources are increased to 200 amperes, the deposition rate of the microlaminated Ti/TiN coating increases to 5  $\mu\text{m/hr}$  (**Table 2**, item G12). This coating, deposited during a ten hour deposition process, has a total thickness of 50  $\mu\text{m}$ . The morphology of this coating is coarser than that of similar coatings deposited by a LAFAD process with lower primary arc currents, as illustrated in **Figure 3a**. It exhibits a larger columnar grain structure with sharper boundaries; this can be explained according to the MDTM zone diagram as being caused by much higher substrate temperature during deposition of this coating, due to higher ion currents generated by the primary arc sources of the LAFAD plasma source. It can also be seen that the bi-layer period in this coating architecture changes from ten microns at the beginning portion of the coating, interfacing the substrate, down to three microns at the top of the coating. This can be explained by a dramatic decrease of the evaporation temperature at the front surface of the targets, and corresponding reduction in evaporation rate, as the targets get shorter due to continuous evaporation. This rate reduction can be compensated for by increasing the primary DCAD source current or by adjusting the evaporation time per each coating bi-layer period. The high adhesive and cohesive strength of this thick microlaminated cermet coating is demonstrated by the Rockwell C 145 kg indentation mark shown in **Figure 3b**. It can be seen that only the bottommost thick ceramic TiN sublayer, interfacing the substrate, in this 50 $\mu\text{m}$  thick microlaminated stack, which experiences the largest mechanical deformation, exhibits the development of a larger lateral crack, while a network of a smaller microcracks are developing mostly in the ceramic sublayers. Using laminated architectures with weak interlayers is a well-known strategy for toughening ceramics [22].

Three monolithic TiN coatings (items H, I and J in **Table 2**), having thicknesses ranging from 40 to 54  $\mu\text{m}$  and a hardness of about

35Gpa, were deposited on substrates installed on the rotating turntable of the LAFAD-500C batch coating system during 12 to 15 hour deposition runs using the unidirectional LAFAD plasma source. The surface roughness is substantially increased after deposition of these monolithic thick ceramic coatings due to development of large grains, nodules and pits throughout the coating in a sharp contrast with the microlaminated cermet G12 coating. The typical cross sections of the coatings marked H12 (deposited with 140 amperes primary cathodic arc current) and J12 (deposited with 200 amperes primary cathodic arc current) are shown in **Figure 4a,b**. It can be seen that coating H12, deposited with lower primary cathodic arc current, shows finer morphology with thinner columns and less sharp interfaces than coating J12 deposited with 200 amperes primary cathodic arc current. This is because of the higher intensity of ion bombardment during the LAFAD coating deposition process at 200 amperes in agreement with the MDTM zone diagram, similar to the above-mentioned microlaminated coatings.

LAFAD technology combines the capability of depositing thick, but extremely hard, ceramic and cermet coatings having various multilayer architectures with nearly defect-free, atomically smooth morphology as illustrated in **Figure 2**. This coating morphology is in sharp contrast with the conventional direct (non-filtered) cathodic arc coating that has a large density of macroparticles, holes, and growth defects which create a large number of ridges and bumps on the surface. The defects in conventional coatings range in size from submicron to 20  $\mu\text{m}$  [7,11]. Multilayer LAFAD coatings, having ductile metallic sublayers followed by superhard ceramic sublayers, provide a desirable combination of soft plastic metal vs. hard and brittle ceramic properties which are optimized to achieve the best erosion resistance in heavy particulate impact conditions. The defect-free LAFAD coatings have neither inclusions nor porosity, and have nearly theoretical maximum density, resulting in high resistance against corrosion and chemical attacks both at ambient conditions and at high temperatures.

The extremely smooth surface and high surface energy of LAFAD cermet coatings protect the components from fouling and deposition, by preventing both mechanical and chemical bonding to any deposited foreign particles. The roughness of the 20+  $\mu\text{m}$  Ti/TiN coated Ti6Al4V plates vs. their pre-deposition roughness (results of different finish pre-treatments) is shown in **Table 1**. It can be seen that these coatings do not increase the initial roughness of the substrate and, in some cases – depending on coating architecture, pre-deposition finish and LAFAD coating deposition process parameters – effectively reduce the initial substrate roughness. The ultra-thick nano-microlaminated Ti/TiN coating designated as coating “K” in **Table 2**, was deposited by a LAFAD source during a ten hour run at 200 amperes total primary cathodic arc source current. The SEM images of the surface of coating “K” and its cross-section are shown in **Figure 5**. This coating consists of  $\sim 0.8\mu\text{m}$  TiN sublayers followed by <100nm metallic titanium sublayers. This coating exhibits a columnar morphology similar to coatings deposited by ionized EB-PVD and ionized magnetron deposition processes [7,11], but with extremely low defect density. Surface roughness did not change after deposition of this ultra-thick cermet coating on samples subjected to bead blasting prior to the LAFAD coating deposition process.

Coating “K” was also deposited as a top segment on Ti64 and 17-4PH steel samples previously coated with either a microlaminated coating, designated as “G” or with one of two monolithic coatings: “P” and “J” (see **Table 2**), forming two-segment coating architectures designated as GK (G+K), IK (I+K) and JK (J+K) coatings. The

characteristic properties of these coatings are presented in **Table 2**. The hardness and elastic modulus of these coatings basically resemble those of coating “K”; the roughness and defect density is much greater for the JK and IK coatings than that of the GK coating, which can be explained by larger roughness, more coarse columnar morphology and more imperfections in monolithic I and J coatings compared to the microlaminated G coating. The SEM image of the cross section of the GK coating in **Figure 6** shows the two-segment architecture with microlaminated bottom G segment and nanolaminated top K segment coating. The density of defects in this coating does not exceed 10 per 100x100 $\mu$ m area. In addition, these defects are localized inside of the coating and do not extend across more than a few sublayers. The morphology of the top segment of the GK coating is basically similar to that of the K coating shown in **Figure 5**. The width and shape of the columns in this coating may be explained by the MDTM zone diagram assuming that the temperature of the surface during the LAFAD deposition process does not exceed 600-700°C, which was also verified by independent assessment. In this temperature range, the morphology of the coatings deposited by ionized atomic condensation is related to zone I of the MDTM zone diagram [11]. High deposition temperature during the LAFAD process even at low bias (<40 volts) can be explained by the large density of ion current conveyed from the vapor plasma to the substrate surface during the LAFAD process.

#### *Erosion resistance performance evaluation*

The microlaminated Ti/TiN coatings B through F deposited by the LAFAD process in the industrial scale batch coating system on substrates made of Ti6Al4V alloy with four different pre-deposition finishing treatments (described above in the “Experimental Details” section), were subjected to erosion testing in the wind tunnel facility at the University of Cincinnati. These coatings had a moderate thickness ranging from 20 to 25  $\mu$ m as outlined in **Table 1**. The tests were conducted using runway sand as the erosion media at 700 fps with a 90° impact angle at ambient temperature. The results of these tests are presented in **Figure 7**. It can be seen that bead blasting finishing provides a dramatic improvement in erosion resistance compared to other types of pre-deposition finishing treatments.

Based on the results obtained during the 700 fps, 90° impact angle testing, all of the subsequent tests were concentrated on samples which had been subjected to bead blasting pre-deposition finishing treatment. Coatings B through F, having bead blasting pre-deposition finishing, were tested in the wind tunnel test facility at the University of Cincinnati using runway sand as the erosion media at 1200 fps with 90° and 25° impact angles at 500°F. The 90° impact erosion results (**Figure 8**) demonstrate that all coatings outperformed the uncoated Ti64 samples for both  $Q_p=2.5$  and  $Q_p=5g$ , while at  $Q_p > 10g$  the coatings’ protective effect is gone. The best coatings (B22 and F22) have more than five times lower erosion rate compared to baseline uncoated titanium for  $Q_p=2.5g$ , while coating B22 still outperformed the baseline by a factor of two for  $Q_p=5g$ .

The erosion resistance performance of all the coatings B through F, which were subjected to bead blasting pre-treatment, improved dramatically in 25° impact angle testing as illustrated in **Figure 8**. Samples with two types of pre-deposition finishing treatment were used in this test: pre-deposition polishing with surface finish RMS < 0.1 $\mu$ m (samples B21 through F21) and bead blasting with RMS  $\approx$  0.8 $\mu$ m (samples B32 through F32). In this case, the best coatings outperformed the baseline by more than a factor of ten for  $Q_p < 5g$  (coatings E and F) and still outperformed the uncoated titanium samples by more than a factor of four for  $Q_p=15g$  (coatings E and F). It can be also seen that samples with polishing pre-treatment still

substantially outperformed the baseline in the entire range of tested  $Q_p$  from 2.5 to 15g (coatings C and D), but they performed worse than samples B32-F32 with bead blasted pre-treatment. This can be explained by the fact that in oblique impacts, the substrate-to-coating interface does not contribute as much to the coating resistance to delamination as that of 90° impacts due to much smaller value of the momentum component perpendicular to the sample surface in 25° impact vs. 90° impact. These results are in agreement with the results of testing G12 50  $\mu$ m thick microlaminated Ti/TiN coating with a large thickness of both metallic Ti and ceramic TiN sublayers (**Table 2**). The results of this testing, which was performed under the same conditions as the tests shown in **Figure 8** (runway sand, 1200 fps, 500°F) at 25° and 90° impact angles, reveal that a microlaminated architecture with large metallic sublayers is less resistant to erosion than architectures with submicron size metallic sublayers even when the overall thickness of this coating is almost two times greater than that of coatings B through F. Only in oblique impact conditions at  $Q_p < 5g$  did this coating outperform the baseline as illustrated in **Figure 9**.

The results of testing the monolithic TiN coatings (**Table 2**, items H12, I12 and J12) with thicknesses ranging from 40 to 54  $\mu$ m are presented in **Figure 9**. These tests were also performed using runway sand at 1200 fps and at 500°F in the wind tunnel testing facility of the University of Cincinnati. All these tests were performed using an erodent mass  $Q_p = 10g$ . It can be seen that all coated samples outperformed the uncoated titanium. The monolithic ceramic coatings’ erosion resistance performance at oblique impacts is substantially better than the 90° impact results, which is a well-known phenomenon with ceramic materials [2,4,23]. Coating I12 was deposited at 200 amperes of primary cathodic arc current in the LAFAD dual arc plasma source as compared to the 140 amperes that was used during the deposition of the J12 coating. This resulted in a coarser columnar morphology of the I12 TiN ceramic coating as compared to the J12 coating, which may have contributed to the better erosion resistance performance of the I12 coating.

The results of testing the ultra-thick TiN coatings at UC were compared to the less aggressive testing at UDRI and screen testing at Arcovac using fine erosion media at relatively low impact speeds. Preliminary investigation of erosion mechanisms of thick TiN coatings with different architectures deposited by the LAFAD process (see **Table 2**) were conducted by subjecting several samples with different coatings to a high speed dust-air jet using a modified FALEX-1507 erosion test rig. In this test, the total mass losses of samples G12, H12, I12 and J12 were a factor of two to three less than the uncoated Ti64 sample and sample I12 showed the best performance in good agreement with the results of a much more aggressive test using runway sand at 1200 fps (**Figure 9**). Better performance of the monolithic nitride-based ceramics vs. cermets was also found in comparative erosion testing reported in [23].

The best erosion resistant performance in wind tunnel testing at UC was demonstrated by a nano-microlaminated Ti/TiN coating designated as coating “K” in **Table 2** with a thickness of approximately 50  $\mu$ m. This coating (as well as the two-segment coatings GK, IK and JK with G, I or J bottom segment coating and K top segment with total thickness 100+  $\mu$ m) dramatically outperformed uncoated titanium during oblique impact (30 degrees) testing as illustrated in **Figure 10**. It has to be noted that in all of the 30-degree tests, the coating was never completely eroded away and hence the substrate never got exposed; this is why the measured erosion rates for  $Q_p = 5$  grams and for  $Q_p = 10$  grams are so very similar. The results of 90° impact testing in the wind tunnel were

less favorable (as would be expected for ceramic coatings) and are not shown in **Figure 10**. The erosion testing results in less aggressive testing at UDRI have demonstrated the exceptionally low wear rate of the nano-microlaminated K coating as well as 2- segment GK, IK and JK coatings. Based on mass loss, the estimated thickness losses were about 12  $\mu\text{m}$  for JK coating tested at 30 deg impact angle and 38  $\mu\text{m}$  at 60° impact angle, weigh below the coating thickness. Thickness measurements of the 30 deg samples using an optical profilometer revealed actual losses that were lower than these estimates, about 7.6  $\mu\text{m}$  (courtesy of K.W.Young, Boeing IDS Rotorcraft).

## SUMMARY

The unidirectional dual arc LAFAD vapor plasma source has been characterized as a generator of high-density ion current and mass flow. The productivity of the LAFAD plasma source is comparable to, or exceeds, the productivity of conventional DCAD sources and magnetron sputtering sources for deposition of thick TiN based erosion protective coatings of different architectures tested and evaluated in this study. For example, one LAFAD source can deposit TiN-based coatings on substrates installed on the 0.5 meter diameter rotating turntable of the industrial size batch coating chamber with a productivity of up to 5  $\mu\text{m/hr}$ . These coatings are also characterized by nearly defect-free morphology, and an extremely smooth surface without the growth defects that are typical in DCAD and magnetron processes, such as nodules, large grains, voids and porosity. The hardness of the thick TiN coatings deposited by the LAFAD process ranges from 15 to 35 GPa depending on coating architecture (e.g. monolithic vs. microlaminated). The LAFAD TiN ceramic and cermet coatings having thicknesses up to 100  $\mu\text{m}$  can still provide a smooth surface with roughness  $\text{RMS} < 1\mu\text{m}$ . The thick TiN based coatings deposited by the LAFAD process, both microlaminated Ti/TiN cermet and monolithic TiN ceramics, can provide an order of magnitude improvement of erosion resistance under conditions of impacts with runway sand particulate flow at the speed of 1200 fps. These properties of the LAFAD process make it an attractive alternative to replace conventional plasma PVD processes for a wide range of applications in turbomachinery.

## ACKNOWLEDGEMENT

The authors would like to acknowledge the technical assistance of Recep Avcı and Paul Gannon for carrying out the SEM analysis. Thanks are also due to Victor Lapkovich for assistance during the experimental trials and sample preparations and to Dr.K.W.Young of Boeing IDS Rotorcraft for testing LAFAD erosion resistant coatings. Portions of this research were supported by the United States Department of Defense via Contract No. W911NF-05-2-0016.

## REFERENCES

1. Hamed, W. Tabakoff, R. Wenglarz, "Erosion and Deposition in Turbomachinery," J. Propul. Power, Vol. 22, No. 2, March–April 2006.
2. Jean-Pierre Immarigeon, David Chow, V.R. Parameswaran, Peter Au, H. Saari and Ashok K. Koul, "Erosion Testing of Coatings for Aero Engine Compressor Components," Advanced Performance Materials, Volume 4, Number 4 / October, 1997, p.371-388.
3. V.R Edwards and P.L Rouse. U.S. Army Rotorcraft Turboshaft Engines Sand and Dust Erosion Considerations. Erosion, Corrosion and Foreign Object Damage Effects in Gas Turbines. AGARD CP 558.
4. Tabakoff, W. and Simpson G., "Experimental Study of Deterioration and Retention on Coated and Uncoated Compressor and Turbine Blades," 40th AIAA Aerospace Sciences Meeting & Exhibition, Reno, NV, Jan 14-17, 2002.
5. A.Sue, Surface and Coating Technology, 62 (1993), 115-120.
6. Shanov, W.Tabakoff, Surface and Coating Technology, 86-87 (1996) 88-93.
7. V.P.Swaminathan, R.Wei, D.Gandy, "Nano technology coatings for erosion protection of turbine components", ASME Paper No. GT2008-50713.
8. Goat, C. Erosion Resistance in Metal-Ceramic Multilayer Coatings for Gas Turbine Compressor Applications. 94. Cranfield, Cranfield University.
9. P.Y Yashar and W.D Sproul. Nanometer Scale Multilayer Hard Coatings. Vacuum **55**, 179-190 (1999).
10. Zhao Linruo, "Nanostructured Coatings for Erosion Protection of Engine Components", Seminar on Advanced Coatings and Surface Systems for Application in Aerospace, Marine and Transportation Industries, The Singapore Institute of Manufacturing Technology, 25 February 2003.
11. R.L.Boxman, D.M.Sanders, and P.J.Martin, *Handbook of Vacuum Arc Science and Technology*. Park Ridge, N.J.: Noyes Publications, 1995.
12. Vladimir I. Gorokhovsky, Rabi Bhattacharya and Deepak G. Bhat, Surface and Coating Technology, 140 (2) 2001, pp. 82-92.
13. V.Gorokhovsky, US Pat. No.7,300,559.
14. V. Gorokhovsky, C. Bowman, D. VanVorous, J. Wallace, "Deposition of Various Metal, Ceramic and Cermet Coatings by an Industrial-Scale LAFAD Process", JVST-A, 2009, In Press.
15. V. Gorokhovsky, C. Bowman, P.E. Gannon, D. VanVorous, J. Hu, C. Muratore, A.A., Voevodin, Y.S. Kang, "Deposition and Characterization of Hybrid Filtered Arc-Magnetron Multilayer Nanocomposite Cermet Coatings for Advanced Tribological Applications," Wear 265 (2008) 741-755.
16. R.J. Smith, C. Tripp, A. Knospe, C.V. Ramana, A. Kayani, V. Gorokhovsky, V. Shutthanandan, D.S. Gelles, "Using CrAlN Multilayer Coatings to Improve Oxidation Resistance of Steel Interconnects for Solid Oxide Fuel Cell Stacks," J. Journal of Materials Engineering and Performance, Volume 13, Number 3, June 2004.
17. H. Jehn, G. Reiners, N. Siegel, DIN-Fachbericht (Special Report) 39, Charakterisierung duenner Schichten (Characterization of thin layers), Beuth-Verlag, Berlin, 1993.
18. V. Gorokhovsky, J. Wallace, C. Bowman, P.E. Gannon, J. O'Keefe, V. Champagne and M. Pepi, "Large area filtered arc and hybrid coating deposition technologies for erosion and corrosion protection of aircraft components", In proceedings of 32nd International Conference & Exposition on Advanced Ceramics & Composites, Daytona Beach, FL, January 27–February 1, 2008.
19. Y. H. Cheng, T. Browne, B. Heckerman, J. C. Jiang, E. I. Meletis, C. Bowman, and V. Gorokhovsky, "Internal stresses in TiN/Ti multilayer coatings deposited by large area filtered arc deposition", JOURNAL OF APPLIED PHYSICS **104**, 093502 (2008).

20. H.Kostenbauer, G.A.Fontalvo, M.Kapp, J.Keckes, C.Mitterer, Annealing of intrinsic stresses in sputtered TiN films: The role of thickness-dependent gradients of point defect density, Surf. Coat. Technol. 201 (2007) 4777-4780.
21. K.J.Ma, A.Bloyce, T.Bell, "Examination of mechanical properties and failure mechanisms of TiN and T-TiN multilayer coatings", Surface and Coatings Technology, 76-77 (1995) 297-302.
22. W.Lee and W.J.Clegg, "The deflection of Cracks at Interfaces", Key Engineering Materials Vols. 116-117 (1996) pp. 193-208.
23. G.E.D'Errico, S.Bugliosi, D.Cuppini, Erosion of ceramics and cermets, J. Mat. Proc. Tech. 118 (2001) 448-453.

**Table 1.** Mechanical properties of thick TiN based coatings deposited by LAFAD process.

Pre-deposition treatment	Sample ID	Primary cathodic arc current, amperes	Thickness, $\mu\text{m}$	Deposition rate, $\mu\text{m/hr}$	Number of layers	Sublayer thickness Ti/TiN at substrate interface, $\mu\text{m}$	Pre-deposition/ Post-deposition roughness RMS (Rz), $\mu\text{m}$	Hardness/ Elastic Modulus, Gpa
Polished	B11*	140	21.05	2.2	9	0.99/1.89	0.04/0.09 (0.94)	18.7/280
Bead Blasted	B12	140	21.05	2.2	9	0.99/1.89	0.93/0.83 (4.97)	18.7/280
Tumbled	B13	140	21.05	2.2	9	0.99/1.89	0.24/0.39 (2.65)	18.7/280
Blasted and Tumbled	B14	140	21.05	2.2	9	0.99/1.89	0.63/0.68 (3.91)	18.7/280
Polished	C11	140	20.74	2.1	8	1.18/1.73	0.03/0.23 (1.60)	15.8/242
Bead Blasted	C12	140	20.74	2.1	8	1.18/1.73	0.94/0.88 (5.03)	15.8/242
Tumbled	C13	140	20.74	2.1	8	1.18/1.73	0.22/0.12 (0.87)	15.8/242
Blasted and Tumbled	C14	140	20.74	2.1	8	1.18/1.73	0.56/0.72 (4.33)	15.8/242
Polished	D11	140	22.33	2.3	12	0.96/1.08	0.02/0.13 (1.01)	13.1/220
Bead Blasted	D12	140	22.33	2.3	12	0.96/1.08	1.24/0.97 (5.33)	13.1/220
Tumbled	D13	140	22.33	2.3	12	0.96/1.08	0.18/0.31 (2.15)	13.1/220
Blasted and Tumbled	D14	140	22.33	2.3	12	0.96/1.08	0.69/0.85 (4.88)	13.1/220
Polished	E11	140	25.30	2.5	12	0.68/1.77	0.019/0.07 (0.72)	19.3/301
Bead Blasted	E12	140	25.30	2.5	12	0.68/1.77	0.85/0.79 (5.10)	19.3/301
Tumbled	E13	140	25.30	2.5	12	0.68/1.77	0.25/0.55 (3.60)	19.3/301
Blasted and Tumbled	E14	140	25.30	2.5	12	0.68/1.77	0.53/0.78 (4.95)	19.3/301
Polished	F11	140	22.41	2.2	8	0.83/2.31	0.03/0.36 (2.56)	17.0/273
Bead Blasted	F12	140	22.41	2.2	8	0.83/2.31	0.63/0.64 (3.94)	17.0/273
Tumbled	F13	140	22.41	2.2	8	0.83/2.31	0.23/0.35 (2.71)	17.0/273
Blasted and Tumbled	F14	140	22.41	2.2	8	0.83/2.31	0.27/0.38 (2.44)	17.0/273

**Table 2. Mechanical properties of ultra-thick monolithic, microlaminated and nano-microlaminated TiN based coatings deposited by LAFAD process (all samples were bead blasted prior to coating deposition runs).**

Sample ID	Primary cathodic arc current, amperes	Thickness, $\mu\text{m}$	Deposition rate, $\mu\text{m/hr}$	Number of layers	Pre-deposition/ Post-deposition roughness RMS(Rz), $\mu\text{m}$	Hardness/ Elastic Modulus, Gpa
G	200	50	5.2	11	0.80/0.87 (5.03)	18.7/324
H	200	40	5	Monolithic	0.02/0.6 (3.2)	~35/480
I	200	46	5	Monolithic	0.80/1.6 (10.2)	~35/480
J	140	54	2.5	Monolithic	0.80/1.80 (11.2)	~35/480
K	200	50	5.2	40	0.80/0.87 (5.03)	25/415
G+K		100		2-segments	0.80/0.87 (5.03)	25/415
I+K		96		2-segments	0.80/1.88 (11.28)	25/415
J+K		104		2-segments	0.80/1.80 (9.49)	25/415

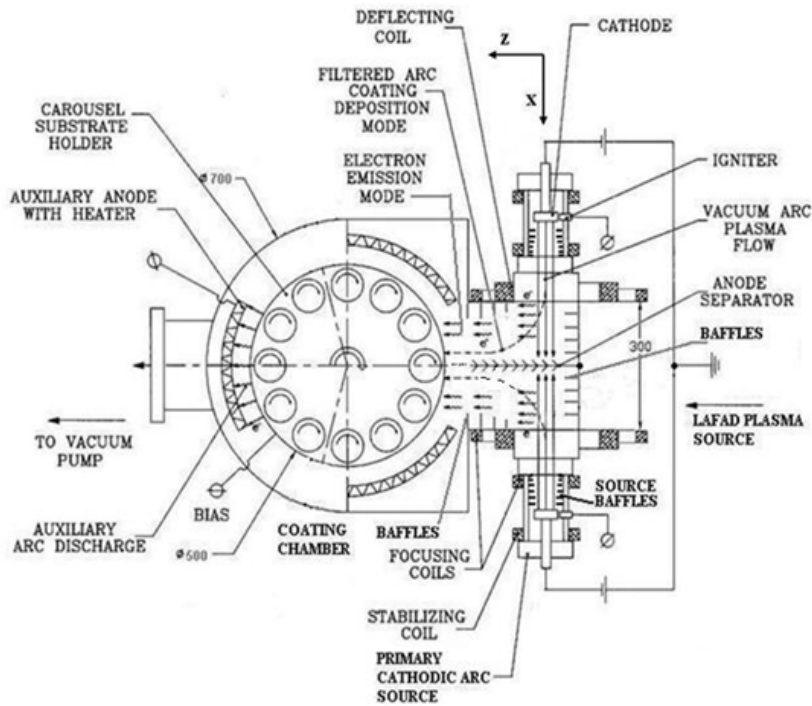


**Figure 1.** Schematic illustration of the LAFAD batch coating system layout in this work (plan view). The unidirectional, dual-arc LAFAD source assembly is to the right; the rotating substrate holder, equipped for dual rotation satellites stations, is shown in the center of the drawing.

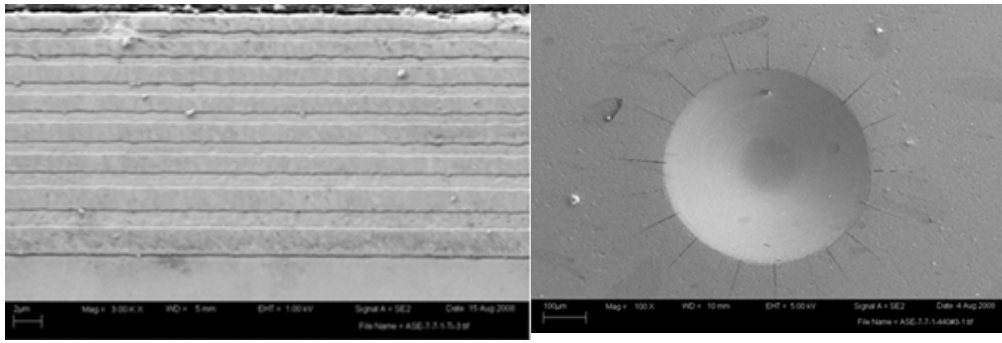


**Figure 2.** SEM images of a 20µm thick Ti/TiN microlaminated LAFAD coating (coating ID: **Table 1**, item C12) deposited during eleven hours of deposition time from one LAFAD source on substrates installed on the rotating turntable of the batch coating system: metallurgical cross-section (left); (b) Rockwell C 145 kg load indentation (right).

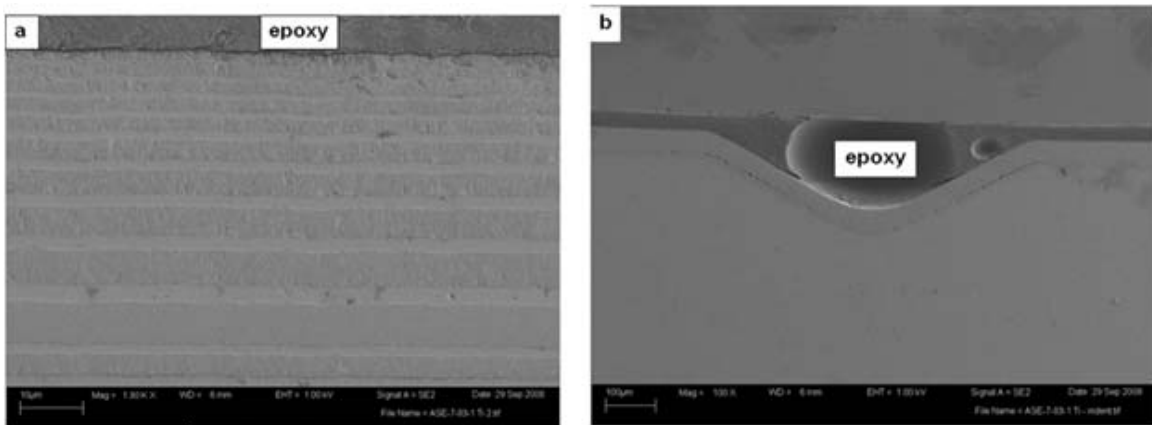


**Figure 3.** The cross-sections of (a) an undamaged portion, and (b) the Rockwell C 145 kg load indentation mark of a 50µm thick Ti/TiN microlaminated coating deposited by one LAFAD source on rotating substrates in the batch coating system during a ten hour deposition time at 200 amperes total currents to the primary titanium DCAD sources (coating ID: **Table 2**, item G12). ((a) is at much higher magnification than (b)).

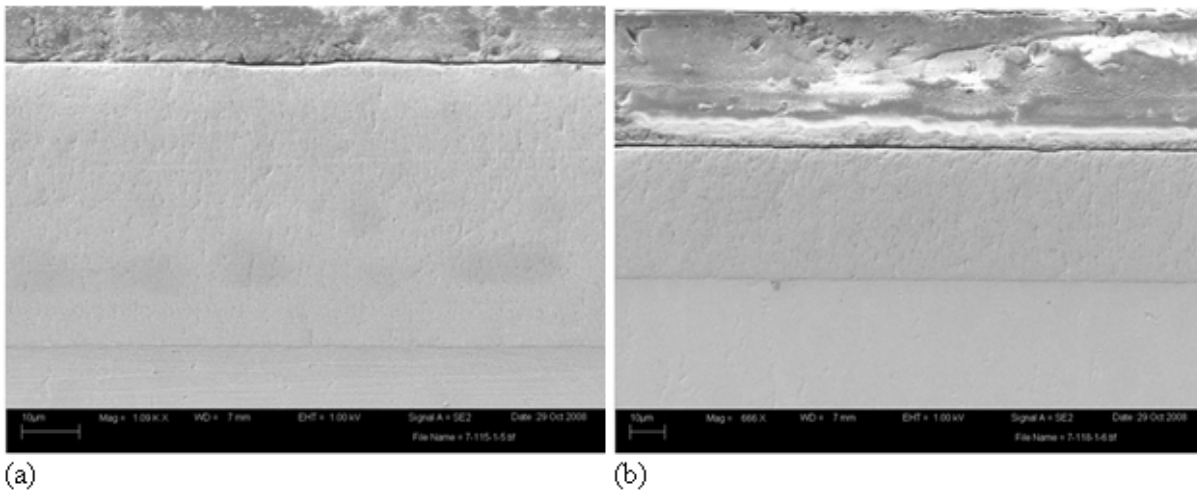


**Figure 4.** SEM cross-section photographs of: (a) sample H12, deposited at 200 Amperes; and (b) sample J12, deposited at 140 Amperes.

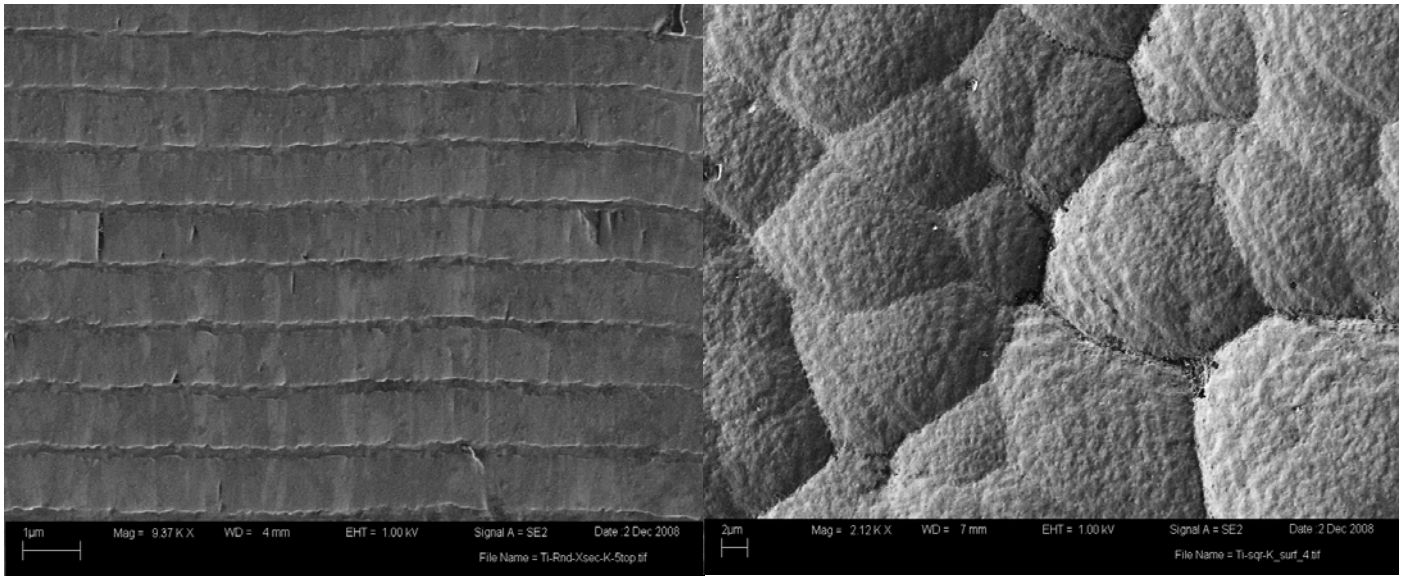


**Figure 5.** SEM photos of coating "K" which was deposited at 200 Amperes for ~ 10 hours. Left = cross-sectional view showing the nano-microlaminated structure; right = top view, showing the columnar microstructure.

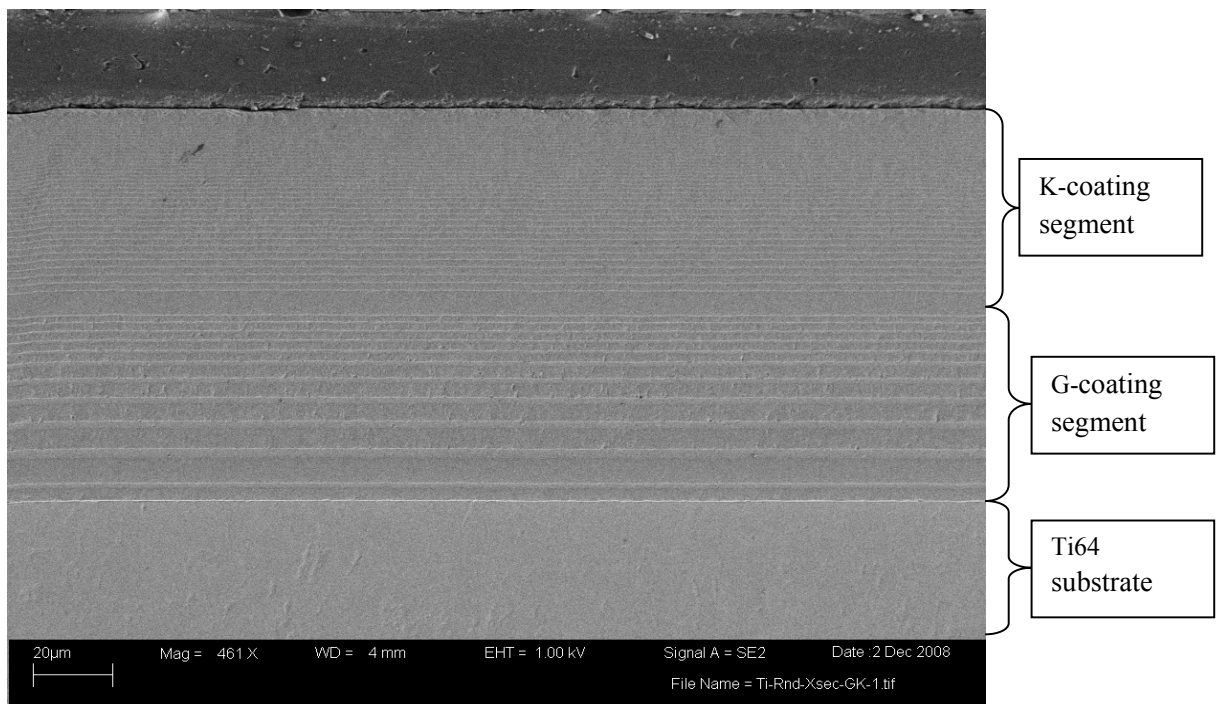


**Figure 6.** SEM cross-sectional view of coating "GK" showing its two-segment architecture.

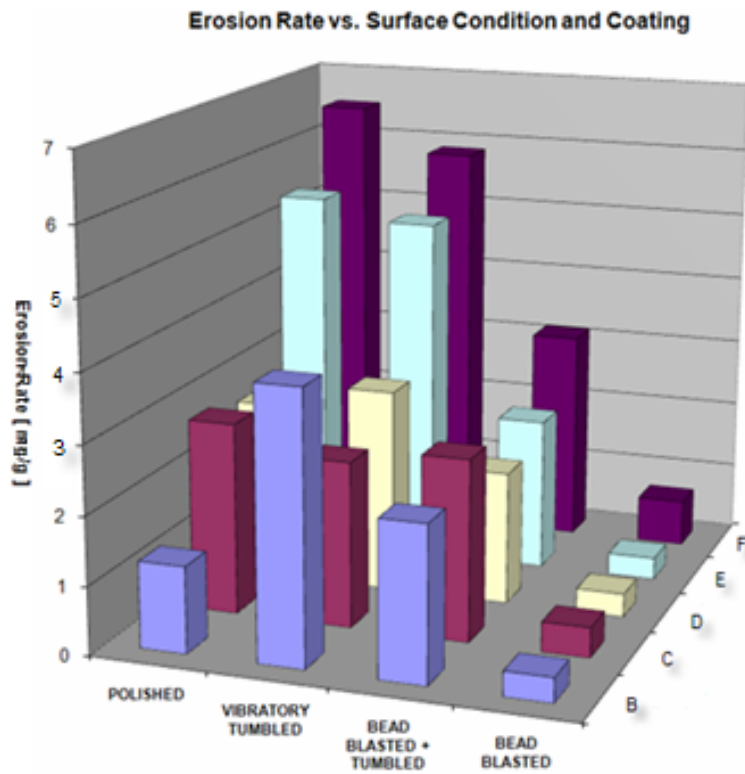


**Figure 7.** Erosion rate of various coated coupons presented in **Table 1** as a function of the surface pre-treatment used (runway sand, 700 fps, 90° impact angle).

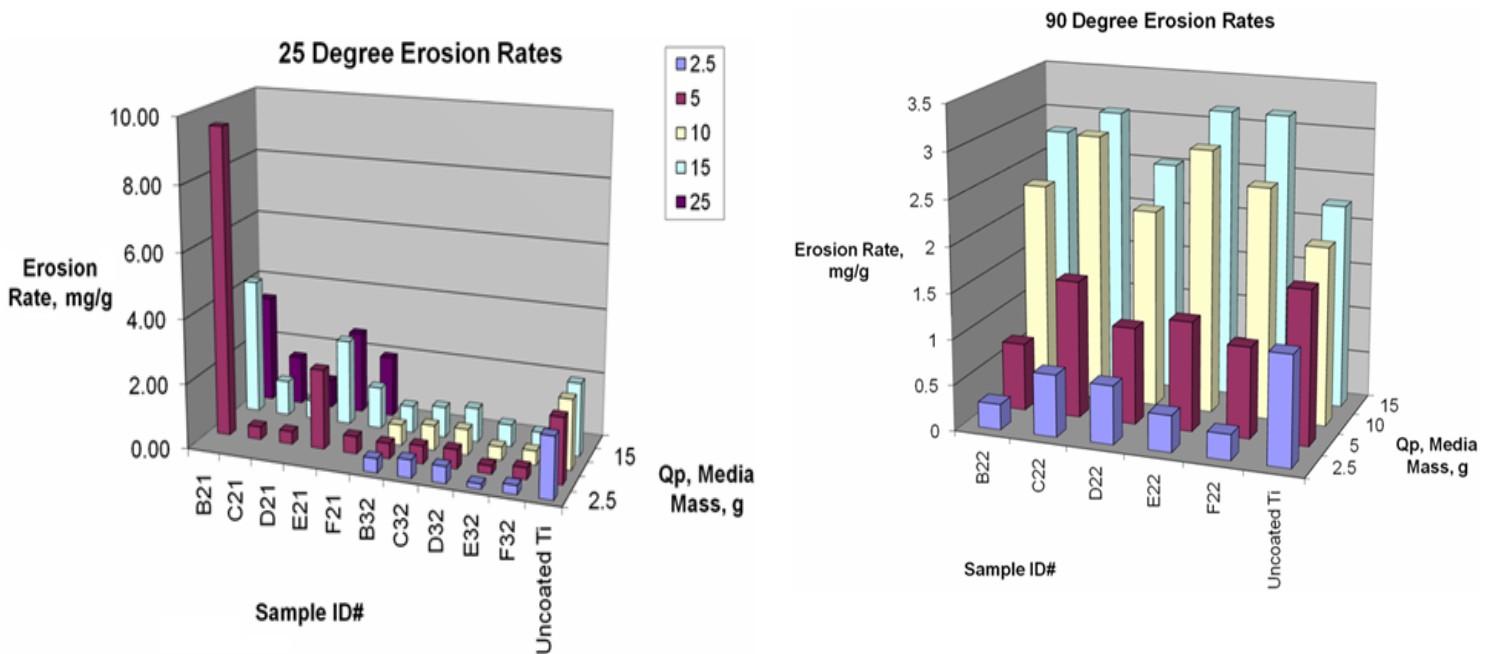


**Figure 8.** Erosion rate of various samples presented in **Table 1**, compared to uncoated titanium, as a function of erodent media mass at a 90° and 25° degree angle of impact (runway sand, 1200 fps, 500°F).

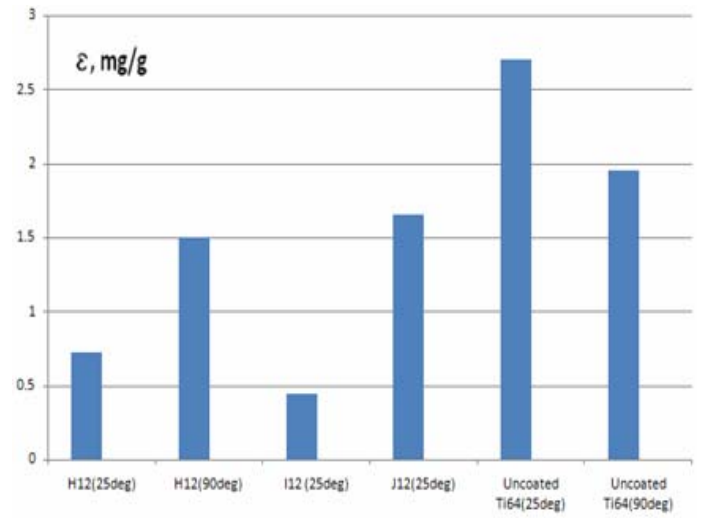
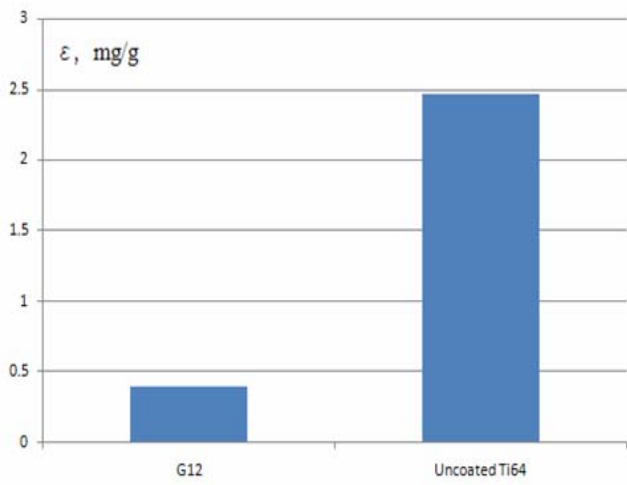


**Figure 9.** The erosion rate of ultra-thick TiN based coatings shown in **Table 2**: sample #G12 with 50 μm thick microlaminated Ti/TiN coating under oblique impact conditions (left), and monolithic TiN coatings H12, I12 and J12 at various angles of impact, compared to uncoated titanium (runway sand, 1200 fps, 500°F).

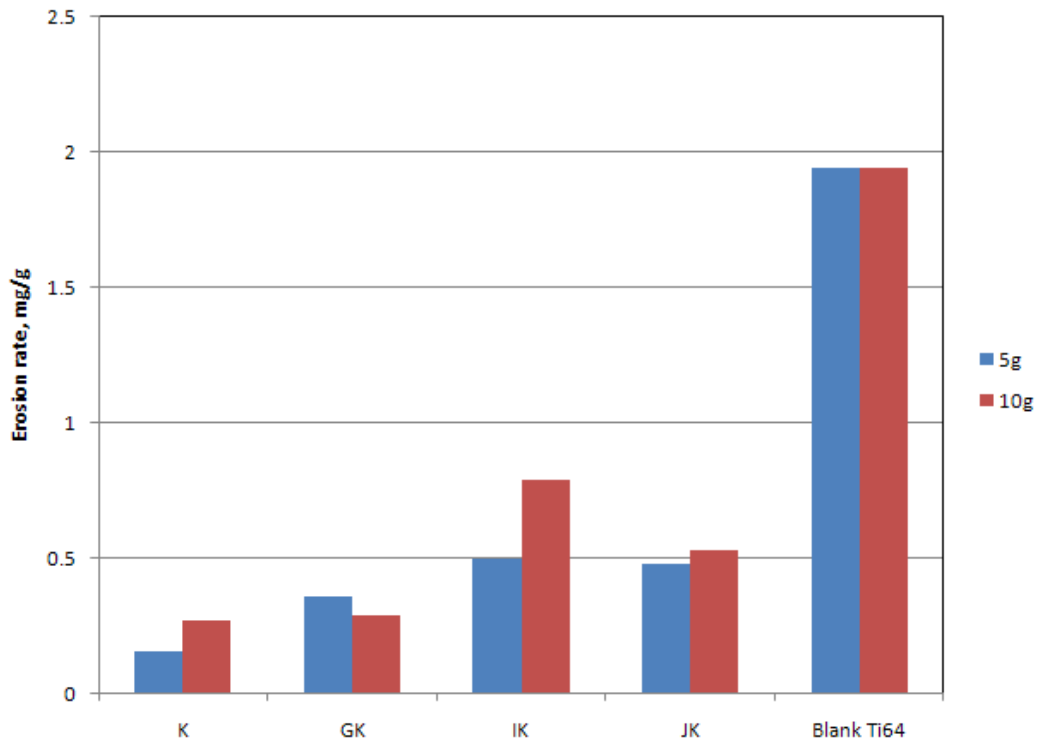


**Figure 10.** Comparisons of the wind-tunnel erosion rates of four different coatings (items K, GK, IK and JK from **Table 2**) compared to uncoated Ti at a 30° impact angle.